EVALUATION OF A COMPACT HELMET-BASED LASER SCANNING SYSTEM FOR ABOVEGROUND AND UNDERGROUND 3D MAPPING

Jianping Li [1], Bisheng Yang [1, *], Yiping Chen [2], Weitong Wu [1], Yandi Yang [1], Xin Zhao [1], Ruibo Chen [3]

[1] State Key Laboratory of Information Engineering in Surveying, Mapping and Remote Sensing, Wuhan University, Wuhan 430079, China – (lijianping; bshyang) @whu.edu.cn
[2] Fujian Key Laboratory of Sensing and Computing for Smart Cities, School of Informatics, Xiamen University, Xiamen 361005, China – chenyiping@xmu.edu.cn
[3] Guangxi Zhuang Autonomous Region Remote Sensing Institute of Nature Resources, Nanning 53000, China – ruiboil@163.com

Commission II, WG II/3

KEY WORDS: HLS (helmet-based laser scanning); ubiquitous point cloud; 3D mapping; SLAM; urban underground space;

ABSTRACT:

As a strategic resource, urban underground space can be used for rail transportation, commercial streets, which has high economic and social benefits, and is of great significance to sustainable city development. Due to denied Global Navigation Satellite System (GNSS) signal, traditional mobile mapping systems have difficulty collecting accurate 3D point clouds in urban underground space. Thus, a helmet-based laser scanning system, named "WHU-Helmet", is integrated in this paper to make up for the shortcomings of the existing traditional mobile mapping systems. "WHU-Helmet" is mainly equipped with four types of sensors: a GNSS receiver (optional), an IMU, a laser scanner, and a global shutter camera. "WHU-Helmet" is not relying on GNSS signal and has the advantages of low cost, small volume and easy operation. Using "WHU-Helmet", a multi-scale Normal Distributions Transform (NDT) based LiDAR-IMU SLAM is implemented to collect underground 3D point cloud in real-time. To validate the performance of "WHU-Helmet" in aboveground and underground 3D mapping, experiments were conducted in a typical urban metro station. The experiments show that the average and RMSE of HLS point errors of "WHU-Helmet" are 0.44 meters and 0.23 meters, respectively, showing great potential of "WHU-Helmet" in the application of aboveground and underground 3D mapping.

1. INTRODUCTION

With the improvement of urbanization, the contradiction between rapid urban development and limited land resources is becoming prominent (Von der Tann et al., 2020). As a strategic resource, urban underground space can be used for rail transportation, commercial streets, and other public infrastructures. Thus, urban underground space has high economic and social benefits, which is of great significance to sustainable city development. Rational utilization of urban underground space, promoting the collective development of aboveground and underground, is a promising solution for improving efficiency use of urban land, reducing urban population density, and expanding capacity of public infrastructure (Qiao et al., 2019). Nevertheless, 3D mapping of the urban underground space is the premise of reasonable planning and maintenance of urban underground resources.

Mobile mapping system (MMS) is one of the most advanced 3D mapping technologies in the field of photogrammetry, and has been widely used in urban infrastructure digitalization (Dong et al., 2018; Mi et al., 2021). Traditional mobile mapping systems (e.g., UAV laser scanning system (Li et al., 2019), car-based laser scanning system (Jaakkola et al., 2010), and et al.) are mainly equipped with two types of sensors, namely, position and orientation system (POS), and laser scanner. Using direct-georeferencing technology (Skaloud and Legat, 2008), the observations of laser scanner could be transformed to the mapping system. However, the POS is relying on the Global Navigation Satellite System (GNSS), and could not be applied in the urban underground space. Long-time and accurate 3D mapping in large-scale GNSS denied underground environment is a research hotspot in both academia and industry (Rouček et al., 2019).

In recent years, a lot of wheeled robot-based systems for 3D mapping in GNSS-denied environments using simultaneous localization and mapping (SLAM) are developed (Chang et al., 2019; Zhang and Singh, 2018). However, the large-weight and high-cost limits the wheeled robot-based mapping system in complex urban underground environments. Wearable mapping systems have the advantages of low cost, small volume and easy operation, which attract attention of the field of photogrammetry (Karam et al., 2020) and robotics (Alliez et al., 2020). Su et al. (2020) developed a backpack laser scanning system, and applied the system in forest inventory successfully. The handheld laser scanning system ZEB developed by GEOSLAM [1] has been applied in several applications, including forest inventory (Camarretta et al., 2021), building information system (Previtali et al., 2019), and protection of ancient buildings (Di Stefano et al., 2021). However, there is still no helmet-based laser scanning system. Thus, a compact helmet-based laser scanning (HLS) system, named WHU-Helmet, is integrated for aboveground and underground 3D mapping of a metro station in this paper.

The remainder of this paper is organized as follows: the hardware description of the HLS system is elaborated in Section 2. A multi-scale Normal Distributions Transform (NDT) based LiDAR-IMU SLAM is implemented in Section 3. In Section 4, the experimental studies are undertaken to evaluate the point cloud accuracy collected by the HLS, after which conclusions are drawn at the end.

---

* Corresponding author

[1] https://geoslam.com/

2. HARDWARE DESCRIPTION OF THE HELMET-BASED LASER SCANNING SYSTEM

2.1 Sensor configuration
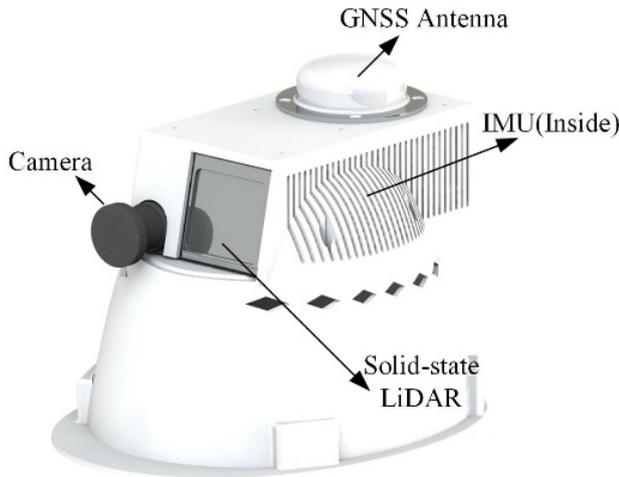
Figure 1. Hardware configuration of the helmet-based laser scanning system, WHU-Helmet.

The WHU-Helmet is composed of four types of sensors: GNSS receiver, MEMS-based IMU, global shutter camera, and solid-state LiDAR. Each sensor is integrated in the HLS as illustrated in Figure 1. The GNSS receiver is used to obtain absolute geo-locations and reference time for the whole system. A micro-electro-mechanical system (MEMS)-based inertial measurement unit (IMU) is used to propagate the system initial position and orientation continuously. A solid-state LiDAR and a global shutter camera are integrated to collect geometry and optical information from the underground environment. Besides, visual and laser features are extracted to constraint the positioning drift of the IMU using SLAM. All the sensors are time-synchronized electronically referencing to the GNSS time according to our previous solution (Li et al., 2019). The total weight of the HLS is about 1.5 kg, which is compact and easy to operate.

2.2 3D mapping system definitions

The 3D coordinate systems involved in the HLS include mapping frame, body frame, and LiDAR frame, which are illustrated in Figure 2. As for a LiDAR observation r_p^l in the LiDAR frame, the corresponding point in the mapping frame could be obtained by:

$$r_p^m = R_b^m(t)R_l^b r_p^l + R_b^m(t)r_l^b + r_b^m(t) \qquad (1)$$

where, $R_b^m(t)$ and $r_b^m(t)$ are the system orientation and position at time t obtained by the SLAM algorithm. R_l^b and r_l^b are the calibration parameters between IMU and the solid-state LiDAR, which are pre-calibrated using similar strategy proposed in our previous work (Li et al., 2020).
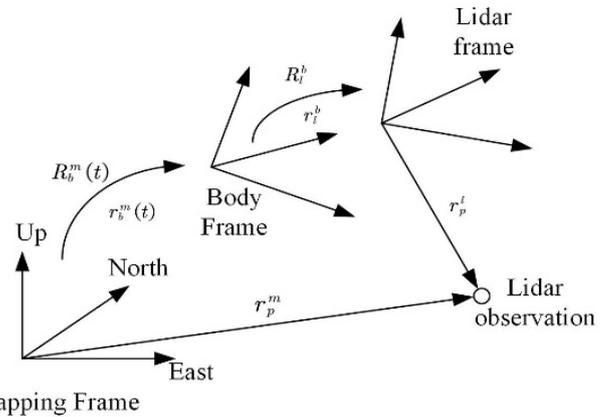
Figure 2. 3D mapping frame involved in the helmet-based laser scanning system.

3. MULTI-SCAL NDT BASED LIDAR-IMU SLAM

The workflow of the proposed multi-scale NDT based LiDAR-IMU SLAM is illustrated in Figure 3. After receiving time-synchronized IMU and LiDAR observations, three steps are involved: (1) IMU pre-integration and correction of motion distortion, (2) Multi-scale NDT based matching and (3) LiDAR and IMU fused optimization, which are detailed as follow:
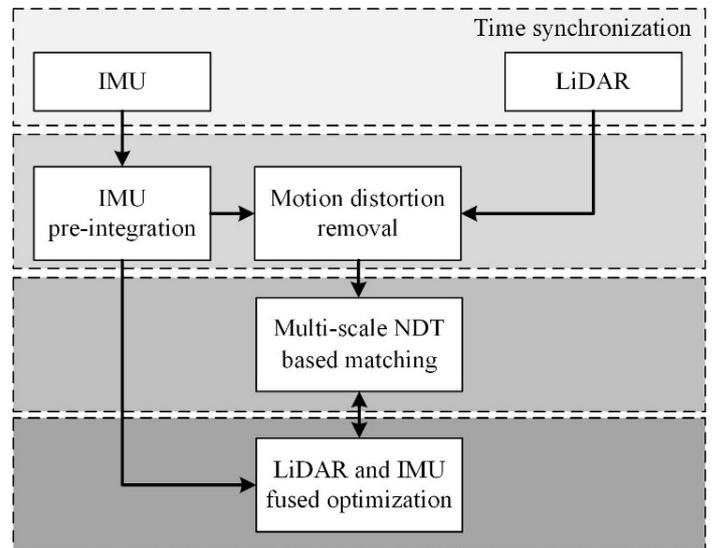
Figure 3 Workflow of multi-scale NDT based LIDAR-IMU SLAM

3.1 IMU pre-integration and correction of motion distortion

As the motion distortion caused by the continuous observation mode of the laser scanner, the IMU measurements collected within the kth laser frame are used to correct the LiDAR motion distortion. The IMU pre-integration model (Qin et al., 2018) is used to calculate the relative motion as follow:

$$
\begin{aligned}
r_b^m(t_{k+1}) = r_b^m(t_k) + v_b^m(t_k)\Delta t - \frac{1}{2}g^m \Delta t^2 \\
+ R_b^m(t_k)^\top \underbrace{\left(\iint_{t \in [k,k+1]} [R_b^m(t_k)(\hat{a}(t) - b_a(t))]dt^2 \right)}_{\alpha_{k+1}^k}
\end{aligned} \qquad (2)
$$

$$v_b^m(t_{k+1}) = v_b^m(t_k) - g^m \Delta t$$
$$+ R_b^m(t_k)^\top \underbrace{\left(\int_{t \in [k, k+1]} [R_b^m(t_k)(\hat{a}(t) - b_a(t))] dt \right)}_{\beta_{k+1}^k} \quad (3)$$

$$q_b^m(t_{k+1}) = q_b^m(t_k) \otimes \underbrace{\int_{t \in [k, k+1]} [\frac{1}{2} \Omega(\hat{\omega}(t) - b_g(t))] dt}_{\lambda_{k+1}^k} \quad (4)$$

where, $\hat{a}(t)$ and $\hat{\omega}(t)$ are the accelerator and gyroscope raw measurements, respectively. g^m is the gravity vector in the mapping frame. α_{k+1}^k, β_{k+1}^k and λ_{k+1}^k are the pre-integration parts, which reflect the relative motion of the short time period during the kth laser frame.

3.2 Multi-scale NDT based matching

NDT is a well-known LiDAR SLAM technology (Magnusson et al., 2007), which transform the point cloud registration problem to optimization the probability density function $f(p)$ as follow:

$$f(p) = \frac{1}{(2\pi)^{\frac{3}{2}} \sqrt{|\Sigma|}} e^{-\frac{(p-\mu)^\top \Sigma^{-1}(p-\mu)}{2}} \quad (5)$$

where, μ is the mean value, Σ is the covariance matrix. As for the solid-state laser scanner equipped in the helmet-based laser scanning system, there are great differences in the point density of the one laser. The point density near the scanning center is large, on the contrary, the point density far away from the scanning center is small. It is hard to decide the voxel size used for NDT. In order to ensure that there are enough points in the distant voxels to accurately calculate the covariance, the voxel size needs to be set large, resulting in the low resolution of the near grid and the loss of the details. Therefore, it is difficult to select the appropriate voxel size to balance the details of near and far voxels.

In this paper, multi-scale normal distribution transformation is adopted to overcome the above problem, as follows: (1) the voxel size is set to S_{voxel} (0.5 m used in the experiment), then calculate the mean value, covariance matrix, point size, eigen vector, and the geometric attributes (linear or planar or irregular)(Magnusson, 2009); (2) Carry out iterative merging of voxels according to the merging conditions listed in Table 1; (3) all parameters in the merged voxels are updated.

Table 1. Voxel merging conditions.

Voxel size after merging is less than $S_{\max}$ (2 m used in the experiment); and
Two voxels are linear before merging, they are still linear after merging; or
Two voxels are planar before merging, they are still planar after merging; or
Two voxels are irregular before merging; or
One voxel is linear, another one is irregular, they are linear after merging; or
One voxel is planar, another one is planar, they are planar after merging; or

3.3 State estimation

In this paper, two kinds of data are used to estimate the state parameters of helmet-based laser scanning system in real time,

namely, IMU pre-integration constraint $e_{Preinte}^{k, k+1}$ and NDT constraint $e_{LiDAR}^{k, k+1}$. NDT constraint $e_{LiDAR}^{k, k+1}$ is similar with existing works (Magnusson et al., 2007).

As for the IMU pre-integration constraints, which are derived according to Eq. (2-4) as follow:

$$e_{Preinte}^{k, k+1} = \begin{bmatrix} \delta\alpha_{k+1}^k \\ \delta\beta_{k+1}^k \\ \delta\lambda_{k+1}^k \\ \delta b_a^k \\ \delta b_g^k \end{bmatrix}$$
$$= \begin{bmatrix} R_b^m(t_k)^\top (r_b^m(t_{k+1}) - r_b^m(t_k) - v_b^m(t_k)\Delta t + \frac{1}{2} g^m \Delta t^2) - \alpha_{k+1}^k \\ R_b^m(t_k)^\top (v_b^m(t_{k+1}) - v_b^m(t_k) + g^m \Delta t) - \beta_{k+1}^k \\ 2[q_b^m(t_{k+1})^{-1} q_b^m(t_k) \otimes \lambda_{k+1}^k]_{1:3} \\ b_a(t_{k+1}) - b_a(t_k) \\ b_g(t_{k+1}) - b_g(t_k) \end{bmatrix} \quad (6)$$

Considering the real-time 3D mapping requirements of the HLS system, sliding window (Huang et al., 2011) is used. The historical laser frame and IMU information are marginalized and transformed into a priori constraints e_{Margin}. These Three kinds of constraints constitute the energy function E, as follow:

$$E = \sum e_{Preinte}^{k, k+1 \top} e_{Preinte}^{k, k+1} + \sum e_{LiDAR}^{k \top} e_{LiDAR}^k + e_{Margin}^\top e_{Margin} \quad (7)$$

Specifically, to solve E, the general least square equation is as follow:

$$H \delta x = b \quad (8)$$

where, H is the Hessian matrix, δx is correction value for system states, b is the error terms. δx is consisted of two parts: $\delta x = [\delta x_{marg}^\top, \delta x_{remain}^\top]^\top$, δx_{marg} is the historical state parameters to be deleted, δx_{remain} is the current state parameters to be estimated. Then we could rewrite Eq. (8):

$$\begin{bmatrix} H_{marg} & H_{remain} \\ H_{remain}^\top & H_{corr} \end{bmatrix} \begin{bmatrix} \delta x_{marg} \\ \delta x_{remain} \end{bmatrix} = \begin{bmatrix} b_{marg} \\ b_{remain} \end{bmatrix} \quad (9)$$

According to Schul complementation, Eq. (9) is rewritten as:

$$\begin{bmatrix} H_{marg} & H_{remain} \\ 0 & H_{corr} \end{bmatrix} \begin{bmatrix} \delta x_{marg} \\ \delta x_{remain} \end{bmatrix} = \begin{bmatrix} b_{marg} \\ b_{remain} - H_{corr}^\top H_{marg}^{-1} b_{marg} \end{bmatrix} \quad (10)$$

Without solving δx_{marg}, δx_{remain} is solved with considering historical constraints. The marginalization term e_{Margin} is obtained as follow:

$$e_{Margin} = H_{corr} \delta x_{remain} + b_{remain} - H_{corr}^\top H_{marg}^{-1} b_{marg} \quad (11)$$

4. EXPERIMENTS

4.1 Study area and data collection

The study area as shown in Figure 4 is located in Computer Town Metro Station (30.53 N, 114.36 E), Wuhan City, Hubei Province, China. The operator carried the HLS, and walked at the speed of 1.3 m/s to scan the environment from aboveground to the underground using about 20 minutes. The real-time 3D mapping results are illustrated in Figure 5, Figure 6, Figure 7, and Figure

8, which are rendered according to intensity in the RVIZ [2]. First the operator walked along the roadside to the metro station entrance 1. Then the operator walked into the metro station through the elevator. It took about 10 minutes to collect underground data in the metro station. At last, the operator walked outside the metro station through the metro station entrance 2.

Figure 4. Study area in Wuhan. (a) Location of Computer Town metro station in satellite image; (b) Snapshot of the metro station aboveground; (c) Snapshot of the metro station underground;
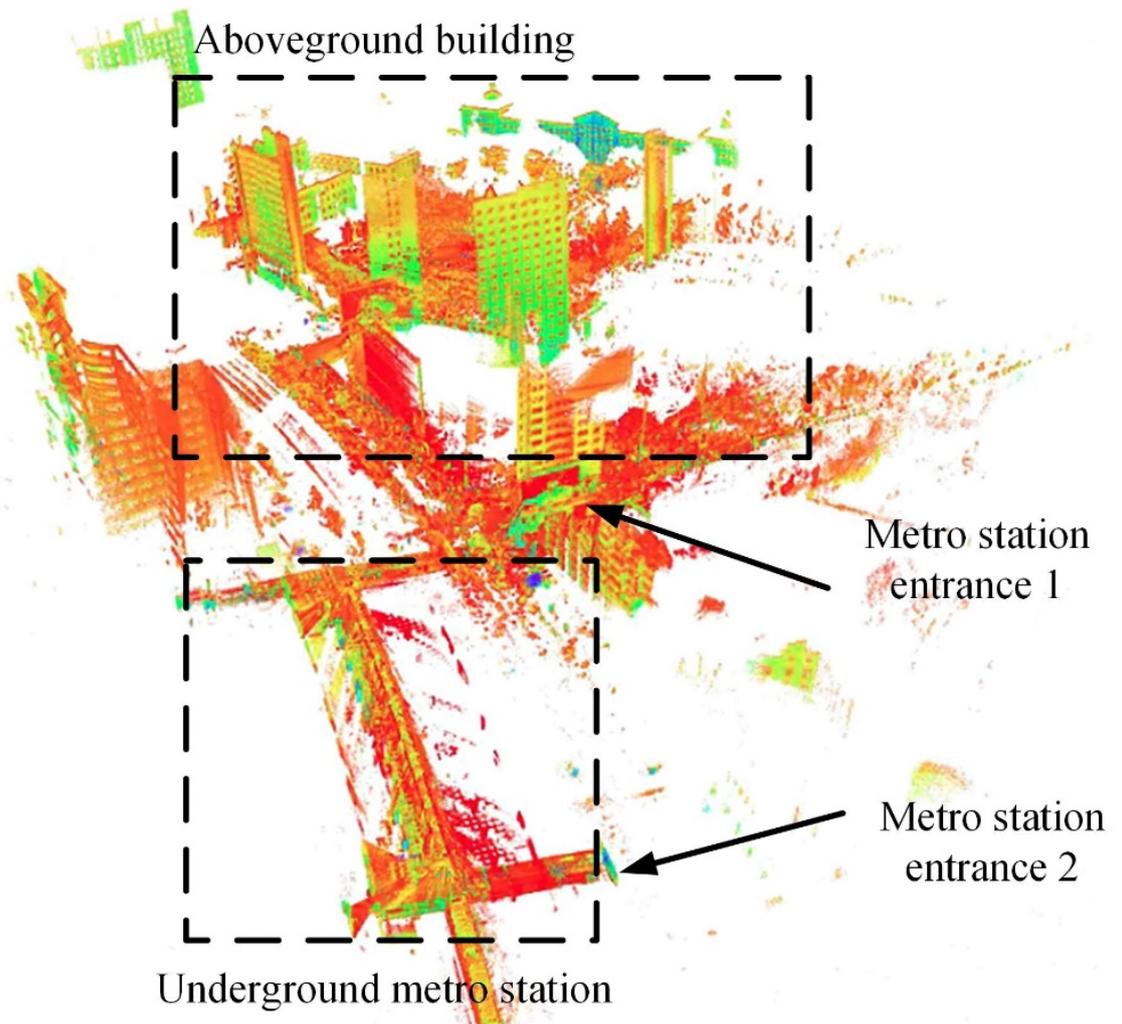
Figure 5 Overview of the aboveground and underground point clouds collected by the helmet-based laser scanning system.

---

[2] http://wiki.ros.org/rviz
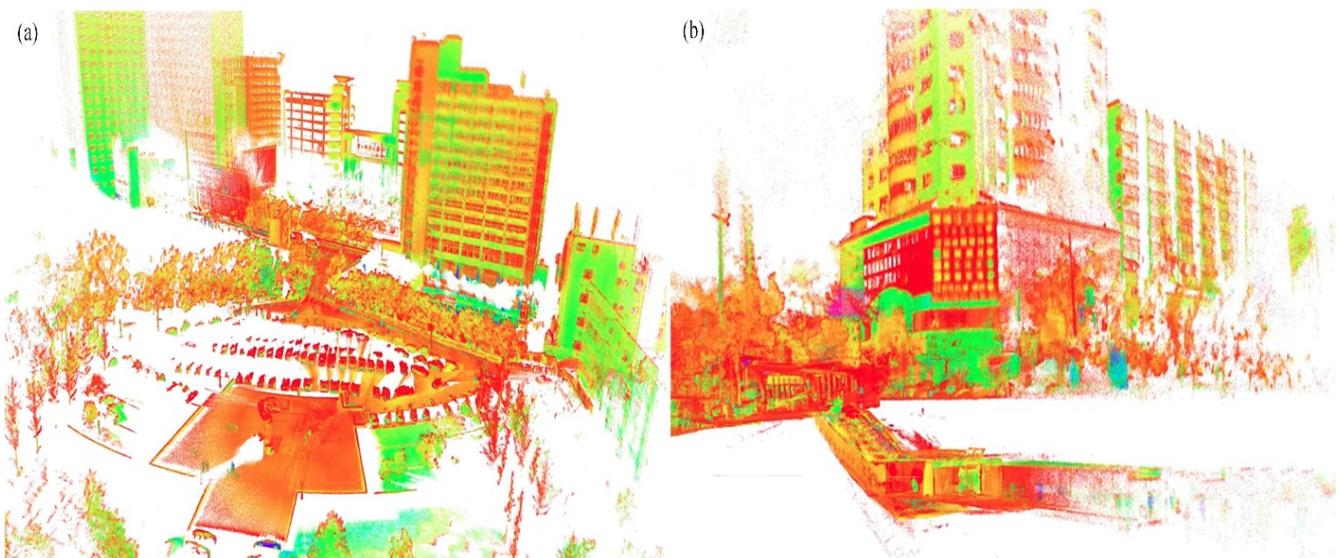
Figure 6 Walking into the metro station. (a) above ground building; (b) the entrance elevator of the metro station.
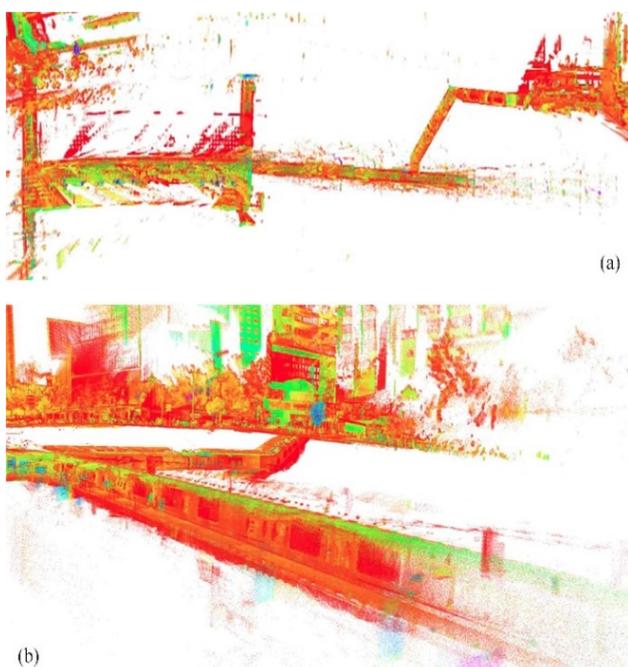
Figure 7 Walking in the metro station. (a) overview of the whole metro station. (b) point clouds inside the metro station

Figure 8. Walking out of the metro station.

4.2 Accuracy evaluation

To validate the geometry accuracy of the HLS in aboveground and underground 3D mapping, point clouds were collected using terrestrial laser scanning (TLS) too. The registered multiple scans from TLS are served as references. 30 evenly distributed corresponding corner points are selected from both TLS point clouds and HLS point clouds. The error distributions of the 30 corresponding corner points are plotted in Figure 9 and listed in Table 2. The average and RMSE of the corresponding point errors are 0.44 meters and 0.23 meters, which has shown a good potential of the HLS for the accurate digitalization of the urban underground space.

5. CONCLUSIONS

Due to denied GNSS signal, traditional mobile mapping systems have difficulty collecting accurate 3D point clouds in urban underground space. In this work, a compact helmet-based laser scanning system, named WHU-Helmet, is integrated and evaluated for the urban aboveground and underground 3D mapping in a metro station. The experiments show that the average and RMSE of HLS point errors are 0.44 meters and 0.23 meters, respectively. 3D modelling of the urban underground space using HLS data will be explored in the near future.

Table 2. The error distribution of the HLS point cloud

Study area	Error distribution			
	MIN	MAX	AVERAGE	RMSE
Metro station	0.19	0.81	0.44	0.23
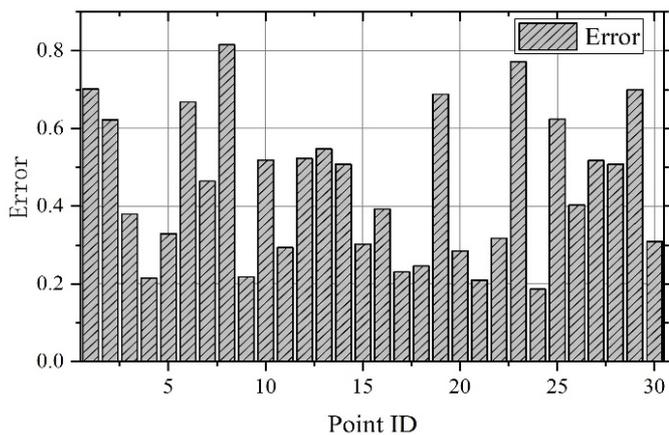
Figure 9 Point clouds accuracy evaluated by terrestrial laser scanning.

ACKNOWLEDGEMENT

REFERENCES

Alliez, P., Bonardi, F., Bouchafa, S., Didier, J.-Y., Hadj-Abdelkader, H., Muñoz, F.I., Kachurka, V., Rault, B., Robin, M., Roussel, D., 2020. Real-time multi-slam system for agent localization and 3d mapping in dynamic scenarios, 2020 IEEE/RSJ International Conference on Intelligent Robots and Systems (IROS). IEEE, pp. 4894-4900.

Camarretta, N., Harrison, P.A., Lucieer, A., Potts, B.M., Davidson, N., Hunt, M., 2021. Handheld laser scanning detects spatiotemporal differences in the development of structural traits among species in restoration plantings. Remote Sensing 13, 1706.

Chang, L., Niu, X., Liu, T., Tang, J., Qian, C., 2019. GNSS/INS/LiDAR-SLAM integrated navigation system based on graph optimization. Remote Sensing 11, 1009.

Di Stefano, F., Torresani, A., Farella, E.M., Pierdicca, R., Menna, F., Remondino, F., 2021. 3D Surveying of Underground Built Heritage: Opportunities and Challenges of Mobile Technologies. Sustainability 13, 13289.

Dong, Z., Yang, B., Liang, F., Huang, R., Scherer, S., 2018. Hierarchical registration of unordered TLS point clouds based on binary shape context descriptor. ISPRS Journal of Photogrammetry and Remote Sensing 144, 61-79.

Huang, G.P., Mourikis, A.I., Roumeliotis, S.I., 2011. An observability-constrained sliding window filter for SLAM, 2011 IEEE/RSJ International Conference on Intelligent Robots and Systems. IEEE, pp. 65-72.

Jaakkola, A., Hyyppä, J., Kukko, A., Yu, X., Kaartinen, H., Lehtomäki, M., Lin, Y., 2010. A low-cost multi-sensoral mobile mapping system and its feasibility for tree measurements. ISPRS journal of Photogrammetry and Remote Sensing 65, 514-522.

Karam, S., Lehtola, V., Vosselman, G., 2020. Strategies to integrate IMU and LiDAR SLAM for indoor mapping. ISPRS Annals of the Photogrammetry, Remote Sensing and Spatial Information Sciences 1, 223-230.

Li, J., Yang, B., Chen, C., Habib, A., 2019. NRLI-UAV: Non-rigid registration of sequential raw laser scans and images for low-cost UAV LiDAR point cloud quality improvement. ISPRS Journal of Photogrammetry and Remote Sensing 158, 123-145.

Li, J., Yang, B., Chen, C., Wu, W., Zhang, L., 2020. Aerial-triangulation aided boresight calibration for a low-cost UAV-LiDAR system. ISPRS Annals of Photogrammetry, Remote Sensing & Spatial Information Sciences.

Magnusson, M., 2009. The three-dimensional normal-distributions transform: an efficient representation for registration, surface analysis, and loop detection. Örebro universitet.

Magnusson, M., Lilienthal, A., Duckett, T., 2007. Scan registration for autonomous mining vehicles using 3D‑NDT. Journal of Field Robotics 24, 803-827.

Mi, X., Yang, B., Dong, Z., Liu, C., Zong, Z., Yuan, Z., 2021. A two-stage approach for road marking extraction and modeling using MLS point clouds. ISPRS Journal of Photogrammetry and Remote Sensing 180, 255-268.

Previtali, M., Banfi, F., Brumana, R., 2019. Handheld 3D Mobile Scanner (SLAM): Data Simulation and Acquisition for BIM Modelling, International Workshop on R3 in Geomatics: Research, Results and Review. Springer, pp. 256-266.

Qiao, Y.-K., Peng, F.-L., Sabri, S., Rajabifard, A., 2019. Low carbon effects of urban underground space. Sustainable cities and society 45, 451-459.

Qin, T., Li, P., Shen, S., 2018. Vins-mono: A robust and versatile monocular visual-inertial state estimator. IEEE Transactions on Robotics 34, 1004-1020.

Rouček, T., Pecka, M., Čížek, P., Petříček, T., Bayer, J., Šalanský, V., Heřt, D., Petrlík, M., Báča, T., Spurný, V., 2019. Darpa subterranean challenge: Multi-robotic exploration of underground environments, International Conference on Modelling and Simulation for Autonomous Systesm. Springer, Cham, pp. 274-290.

Skaloud, J., Legat, K., 2008. Theory and reality of direct georeferencing in national coordinates. ISPRS Journal of Photogrammetry and Remote Sensing 63, 272-282.

Su, Y., Guo, Q., Jin, S., Guan, H., Sun, X., Ma, Q., Hu, T., Wang, R., Li, Y., 2020. The development and evaluation of a backpack LiDAR system for accurate and efficient forest inventory. IEEE Geoscience and Remote Sensing Letters 18, 1660-1664.

Von der Tann, L., Sterling, R., Zhou, Y., Metje, N., 2020. Systems approaches to urban underground space planning and management–A review. Underground Space 5, 144-166.

Zhang, J., Singh, S., 2018. Laser–visual–inertial odometry and mapping with high robustness and low drift. Journal of Field Robotics 35, 1242-1264.